Available online at www.sciencedirect.com
SCIENCE DIRECT®
Solar Energy Materials & Solar Cells
ELSEVIER
Solar Energy Materials & Solar Cells 87 (2005) 181–196
www.elsevier.com/locate/solmat

Optical filters from SiO_2 and TiO_2 multi-layers using sol–gel spin coating method

D. Saygın Hinczewski[a], M. Hinczewski[b,c], F.Z. Tepehan[a], G.G. Tepehan[a,*]

[a]*Department of Physics, Istanbul Technical University, Maslak 34469, Istanbul, Turkey*
[b]*Department of Physics, Massachusetts Institute of Technology, Cambridge, MA 02139, USA*
[c]*Feza Gürsey Research Institute, TÜBİTAK—Bosphorus University, Çengelköy 81220, Istanbul, Turkey*

Received 15 May 2004; received in revised form 30 June 2004; accepted 5 July 2004
Available online 30 November 2004

Abstract

Sol–gel spin coating process is used to produce optical filters from SiO_2 and TiO_2 multi-layers. By coating the films symmetrically on both sides of the glass substrates, we designed two types of three-layer anti-reflective (AR) filters for the near–infrared region, and a nine-layer reflective filter for the near–UV region. We develop a simple theoretical model for these filters, which incorporates sol–gel film densification during the coating process, and fit it to the experimental data to extract properties of the individual layers in the coatings.

Keywords: Sol–gel; Spin coating; Anti-reflective (AR) filter; Reflective filter; SiO_2; TiO_2; Densification model

1. Introduction

Many sol–gel coatings have been reported which have reflective [1–12] and antireflective (AR) [12–19] properties. They vary according to the chosen substrate, sol, central wavelength, number of layers, optical thickness arrangement, coating

*Corresponding author. Tel.: +90 212 285 3219; fax: +90 212 285 6386.
E-mail address: tepehan@itu.edu.tr (G.G. Tepehan).

0927-0248/$ - see front matter
doi:10.1016/j.solmat.2004.07.022

technique, and firing details. Compared to physical and chemical vapor methods, the sol–gel method is inexpensive and easily adaptable to industry scale and mass production. It is possible to work in normal atmospheric conditions and get high homogeneity of the final coatings. The process can be controlled by temperature or through the chemical contents and their molar ratios. There are a variety of options for depositing the coatings, namely spinning, dipping or spraying the substrate with the sol.

In this paper, a nine-layer near–UV reflective and two types of three-layer near-infrared (NIR) AR filters were obtained by using a sol–gel spin coating method on both sides of the glass substrate. For the reflective filter alternating high-index TiO_2 and low-index SiO_2 layers were deposited, while for the AR filter, an additional layer, a TiO_2–SiO_2 mixture, was used as a medium-index. TiO_2 and SiO_2 were chosen because of their high index contrast and their resistance to corrosion.

One of the major goals in the design of the sol–gel optical filters is to be able to predict the behavior of the total system based on the properties of the individual layers in the coating. While it is easy to determine the refractive index and thickness of a single layer deposited on a substrate, using these properties to estimate the actual index and thickness of the layer when it is part of a multi-layer stack is significantly harder. Due to the nature of the multi-layer coating process, one layer may experience longer durations of heat treatment than another, and thus there are varying degrees of densification for layers at different positions along the stack. We have developed a theoretical model for our double-sided multi-layer systems, which is sophisticated enough to approximately account for this densification, yet simple enough to give reliable, physically sensible results when fitted to the experimental data.

2. Theoretical model

We construct a simple theoretical model in order to examine the optical properties of the component layers in our filter systems, and verify that the experimental results from the multi-layer films are consistent with what we expect from our single-layer measurements. Given the thickness, refractive index $n(\omega)$, and extinction coefficient $k(\omega)$, of each layer in our system, we want to calculate the total reflectance and transmission as a function of wavelength, so as to compare them to the spectrophotometer results. Both the reflective and AR filter systems consist of a glass substrate coated on both the sides. Proceeding from inside out, the sequence of layers on each side is identical.

The passage of a beam through such a system is shown schematically in Fig. 1. Since the total thickness of the multi-layer films C and C' on either side $\sim 10^2$–10^3 nm, which is the same order as the wavelength of the incident light, the multiple reflected and transmitted beams as the light passes through the film are essentially coherent. On the other hand, the thickness of the substrate is $\sim 10^6$ nm, so beams whose path difference involves one or more traversals through the substrate will be treated as incoherent. The reflection and transmission coefficients r_1 and t_1,

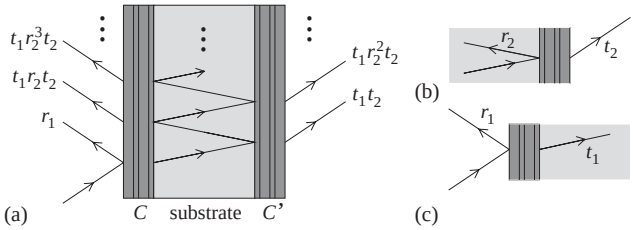

Fig. 1. Part (a) of the figure shows the substrate with a series of layers C and C' on either side, where C' is the same as C in reverse order. The reflection coefficients for beams contributing to the total R are shown on the left, and the transmission coefficients for beams contributing to the total T on the right, in terms of the reflection and transmission coefficients r_1, r_2, t_1, t_2, defined in parts (b and c).

for a beam passing through our multi-layer stack from outside in, can be easily determined through the standard transfer matrix method [20]. The same is true for r_2 and t_2, for a beam passing through the film from inside out. Thus r_1, r_2, t_1 and t_2 will be some functions of the thicknesses, $n(\omega)$, and $k(\omega)$ of the individual layers. The reflection and transmission coefficients for beams making multiple passes through the substrate are just products of r_1, r_2, t_1, and t_2, as shown in the figure. To find the total R and T, we sum the coefficients of the series of beams incoherently:

$$R = |r_1|^2 + \sum_{n=0}^{\infty} |t_1 r_2^{2n+1} t_2|^2 = |r_1|^2 + \frac{|t_1 r_2 t_2|^2}{1 - |r_2|^4}, \tag{1}$$

$$T = \sum_{n=0}^{\infty} |t_1 r_2^{2n} t_2|^2 = \frac{|t_1 t_2|^2}{1 - |r_2|^4}. \tag{2}$$

We thus can calculate R and T given the thicknesses, refractive indices, and extinction coefficients of the layers.

One additional factor needs to be taken into account before Eqs. (1) and (2) can be usefully applied to model our experimental results. Every time the light passes from one side of the substrate to the other, its intensity is approximately reduced by a factor of $\delta(\omega) = \exp(-\alpha_{\text{sub}}(\omega) d_{\text{sub}})$, where $\alpha_{\text{sub}}(\omega)$ and d_{sub} are the absorption coefficient and thickness of the substrate, respectively. Even a small increase in $\alpha_{\text{sub}}(\omega)$, for example in the near–UV region of the spectrum, will translate into a significant intensity loss because of the large size of $d_{\text{sub}} \approx 10^6$ nm. In the presence of this absorption, every $|t_1|^2$ and $|r_2|^2$ in Eqs. (1) and (2) gets a factor of δ, and the formulas for R and T become

$$R = |r_1|^2 + \frac{\delta^2 |t_1 r_2 t_2|^2}{1 - \delta^2 |r_2|^4}, \tag{3}$$

$$T = \frac{\delta |t_1 t_2|^2}{1 - \delta^2 |r_2|^4}. \tag{4}$$

To determine $\delta(\omega)$, we look at the reflectance and transmission for an uncoated substrate in the spectrophotometer. The R and T data is fitted to a version of Eqs. (3) and (4), with r_1, t_1, r_2, and t_2 simple constants for the case of no layers. From this we get a value for δ at each of the measured wavelengths, and we interpolate to get a function over the entire wavelength range. The resulting form for δ for $\lambda = 300-1000$ nm is shown in Fig. 2. The main effect of this absorption for our systems will be in the $\lambda < 350$ nm region.

To complete our description, we need to choose specific forms for the refractive indices and extinction coefficients of the individual layers in the multi-layer coating. For the refractive index, we use the Wemple–DiDomenico single-effective-oscillator model [21],

$$n^2(\omega) = 1 + \frac{E_d E_0}{E_0^2 - (\hbar\omega)^2}, \tag{5}$$

where E_0 and E_d are parameters describing the oscillator energy and oscillator strength, respectively. This form was found to fit, to a good approximation, a wide variety of materials, including the oxides used in our systems [21]. The values for E_0 and E_d for each layer in our stack will be based on the single-layer results (each type of film used in our system is also prepared separately on the substrate, and the refractive index and extinction coefficients are determined from the spectrophotometer data using standard techniques).

To model the extinction coefficient $k(\omega)$, we note that for the materials in our system, the absorption is almost zero for most of the wavelength range 300–1000 nm, where data was collected. Only in the near–UV region do we expect significant absorption, and this primarily from the layers containing TiO_2, which has an optical band gap around 3.2 eV [22]. To model $k(\omega)$, we assume the onset of optical absorption for each layer is described by the typical relation

$$\alpha(\omega)\hbar\omega = B(\hbar\omega - E_g)^\eta, \tag{6}$$

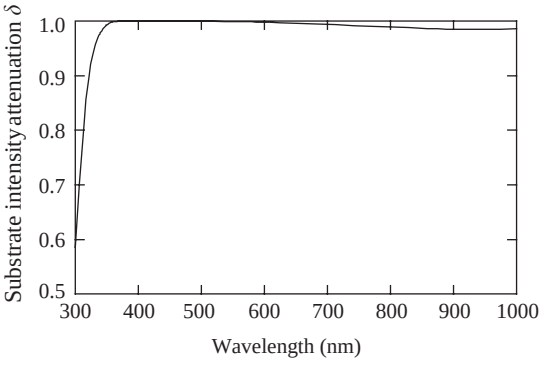

Fig. 2. The intensity attenuation factor $\delta = \exp(-\alpha_{sub} d_{sub})$ for the Corning 2947 glass substrate used for the multi-layer coatings in this study.

where the absorption coefficient $\alpha(\omega) = 4\pi k(\omega)/\lambda$, E_g is the optical band gap energy, B is some constant, and η depends on the kind of optical transitions occurring [23]. For the materials used in our system, we expect indirect transitions and set $\eta = 2$ [22]. Eq. (6) then gives us a simple model for $k(\omega)$,

$$k(\omega) = \frac{cB}{2\hbar\omega^2}(\hbar\omega - E_g)^2\theta(\hbar\omega - E_g) \tag{7}$$

with two parameters E_g and B. Here θ is a unit step function that makes k zero when $\hbar\omega < E_g$. As in the case of the $n(\omega)$ parameters, the values for E_g and B for each layer will be based on the single-layer results.

Lastly, when we consider multi-layer sol–gel coatings, the nature of the fabrication technique means that bottom layers, which are coated first, will experience more heat treatments than the top layers, coated later. Longer exposure to heat treatment can dramatically reduce the thickness of a sol–gel thin film, as residuals from sol–gel synthesis are removed from the film, the gel network condenses, and porosity decreases [24]. Thus a layer near the bottom of the stack will generally be thinner than the same type of layer toward the top [5]. Because of this densification, we expect the refractive indices and extinction coefficients in our multi-layer system to be somewhat larger than the ones calculated from the single-layer samples (which experienced only one heat treatment). The scaling of the refractive index with density ρ can be approximately described by the Lorentz–Lorenz law [25],

$$\frac{\tilde{n}^2(\omega) - 1}{\tilde{n}^2(\omega) + 2} = \tilde{Q}(\omega)\rho, \tag{8}$$

where the complex index $\tilde{n}(\omega) = n(\omega) + ik(\omega)$ and $\tilde{Q}(\omega)$ is some function dependent on the composition of the material. If we know n and k for some density ρ_0 (for example, from the single-layer results), then we can use Eq. (8) to determine n and k for any other density ρ. Associated with each layer we will introduce a parameter $D = \rho/\rho_0 \geqslant 1$ to describe relative densification: compared to the single-layer sample, how much more dense is the same layer in the final stack. This allows us to account for deviation of the n and k from the single-layer results due to densification of the film during the multi-layer coating process.

To summarize: we have described a model for calculating R and T of our multi-layer system, given certain input parameters describing the individual layers. For example, in our reflective filter, we have alternating stacks of SiO_2 and TiO_2. The free parameters are the thickness d_{SiO_2} and d_{TiO_2} of the individual layers, and the densification factors D_{SiO_2} and D_{TiO_2}. The other parameters are assumed to be fixed by the single-layer results. By varying the four free parameters, we do a least-squares fit of the experimental multi-layer R and T data. For this non-linear least-squares fitting problem, we employ the Levenberg–Marquardt multivariate-regression algorithm, as implemented by Wolfram Research's Mathematica software. The s- and p-polarization data sets are fitted simultaneously, to obtain the thickness and dispersion curves of the individual layers in the stack.

The small number of free parameters was achieved through imposing simple, physical constraints on the system, by using the single-layer experimental data and

assuming n and k scale according to the Lorentz–Lorenz law. An alternative would be to dispense with the densification factors and let E_0, E_d, B, and E_g for each layer also be free parameters. For complex systems such as the multi-layer stack, an excess of free parameters often leads to the fitting algorithm getting stuck in an unrealistic local minima, where R and T are closely fit, but with unphysical results for n, k, or the thicknesses. Experience has shown us that fitting with sensible constraints, and a smaller number of free parameters, is more reliable.

A final note on the theoretical simulation: clearly, one of the main sources of error for our simple model will be the variation of the layer thickness within the stack. Because of small variations in preparation, as well as the above-mentioned densification effects, a TiO_2 layer near the bottom will not have exactly the same thickness as one near the top, or even the corresponding TiO_2 layer on the other side of the substrate. In the model, all the layers of the same material are assumed to have the same thickness; otherwise we would end up with an unmanageable number of free parameters. Thus the best-fit d_{TiO_2} should be seen as the average thickness of a TiO_2 layer in the stack; similarly D_{SiO_2} is effectively an average densification factor. Even with this simplification, we believe our model still manages to capture the essential optical properties of our multi-layer stack system; this is borne out by the fitting results discussed in Section 4.

3. Experimental procedure

3.1. Sol preparation for the reflective filter

The SiO_2 sol was synthesized with tetraethylorthosilicate ($Si(OC_2H_5)_4$, TEOS) [99% Aldrich]. TEOS was mixed with isopropanol (C_3H_8O) [99 + % Aldrich] as solvent, distilled water (H_2O) for hydrolysis and hydrochloric acid (HCl) [37% Merck] as catalyst at 70 °C for 80 min. The molar ratios were $TEOS:C_3H_8O:H_2O:HCl = 1:32:32:0.24$. The TiO_2 sol was prepared in two steps using titanium (IV) butoxide ($Ti[O(CH_2)_3CH_3]_4$, TIVBT) [97% Aldrich]. In the first step, TIVBT, ethanol (EtOH) [99.8% Riedel-deHaën] and acetic acid (CH_3COOH) [100% Merck] were mixed at room temperature for 30 min under the molar ratios $TIVBT : EtOH:CH_3COOH = 1:113.45:1.4$. In the second step, ethanol was added to the solution so that the molar ratios became $TIVBT:EtOH:CH_3COOH = 1:189.1:1.4$. After this, the solution was stirred for 1 h more still at room temperature. Both the SiO_2 and TiO_2 solutions came out homogeneous and transparent.

3.2. Sol preparation for the AR filters

The SiO_2 coating sol was based on the same synthesis method as described for the reflective coatings. But the molar ratios of the reagents this time were $TEOS:C_3H_8O:H_2O:HCl = 1:16:16:0.12$. The TiO_2 sol used in the system is exactly the same as for the reflective coatings. Also by using these two sols, a mixture sol of

80 vol% TiO_2–20 vol% SiO_2 was prepared through stirring at room temperature for 30 min.

3.3. Coating process for the reflective filter

Microscope slides (Corning 2947) with dimensions $2.5 \times 2.5 \times 0.1$ cm were used as substrates each time. After washing with glass detergent and rinsing with water as a precleaning step, the glasses were then ultrasonically cleaned (Bandelin, Sonorex RK100, 35 kHz) for 15 min in ethanol. Later on they were dried in a hot-air stream. In order to get each TiO_2 sub-layer in the reflective filter, the coating was done on both the sides by spinning the TiO_2 solution at 2000 rpm. After that, each film was heat-treated at 100 °C by a microprocessor-controlled furnace (Carbolite, CWF 1100). This coating and heating procedure was repeated after another three times to get the final TiO_2 layer. The SiO_2 layers were obtained through coating both the sides of the pre-films by spinning at 3500 rpm and drying for 5 min at 100 °C. The final sequence of layers on each side of the substrate (proceeding from inside out) is: $(HL)^4$ H, where H is the TiO_2 and L is the SiO_2 layer.

3.4. Coating process for the AR filters

3.4.1. Type I

The sizes of the glasses and cleaning procedure were the same as for the reflective filter. In the creation of a three-layer AR filter, the mixture solution 80 vol% TiO_2–20 vol% SiO_2 was spun at 2000 rpm; this is the medium-index first layer. For the second layer, the total TiO_2 layer was obtained by following the coating procedure for the TiO_2 sub-layer in the reflective filter except that it was repeated five times. The third layer, SiO_2, was spun with the corresponding solution at 4000 rpm. Each of these coatings was heated for 5 min at 100 °C after deposition. The final sequence of layers on each side of the substrate (proceeding from inside out) is: the TiO_2–SiO_2 mix, TiO_2, SiO_2.

3.4.2. Type II

For the second type of AR filter, we used the same sol preparation, coating technique, and layer sequence as for Type I, but the sub-layer of TiO_2 was repeated ten times instead of five. Each of the coatings was heated for 5 min at 100 °C after deposition, and in addition we used the stack-firing method [13]: the completed system was heat-treated at 450 °C for 15 min, and then the sample was switched to another furnace at 230 °C, where it was left for 8 min.

3.5. Single-layer preparation

In order to obtain information about the component layers of our system, which we can then use in our theoretical simulation, each of the individual layers mentioned above for the reflective and AR filters was also prepared alone on a substrate. The preparation technique was exactly the same as the one for the

corresponding layer in the multi-layer system. For layers used in the reflective filter and the Type I AR filter, the single layers were heat-treated at 100 °C for 5 min after deposition. For those used in the Type II AR filter, this heat treatment was followed by the stack-firing method described above.

3.6. Characterization

NKD system spectrophotometer (Aquila Instruments) is used to evaluate transmission and reflection intensity of both single and multi-layer prepared films at an incident angle of 30°. The single layer thickness and refractive indices were determined with the package program PRO-Optix Version 4.3 included in the NKD system; these results were double-checked with our own fitting algorithm. The optical properties of the individual layers within the completed systems were calculated through the theoretical model described in Section 2. The adhesion of the filters was evaluated by cross cut and tape tests. The surface roughness was determined by atomic force microscopy (Shimadzu).

4. Results and discussion

4.1. Reflective filter

The design and material properties of our filter systems were motivated by predictions from our theoretical model: to get a rough sense of how the system behaves, we set the thickness parameters in the model equal to those of the corresponding single layer samples, and made the densification factors all equal to 1. For the reflective filter, the results indicated that maximum reflectance occurred approximately at a wavelength λ where the system satisfied a detuning condition [7]: the sum of the optical thicknesses of the basic unit in our stack, the TiO_2 and SiO_2 layers, was equal to $k\lambda/2$, where $k = 1$. We varied our sol preparation parameters until we found a combination, which would give maximum reflectance for $\lambda \approx 500$ nm, given the thickness values from the single-layer samples. Factoring in thickness reduction during the multiple coating process, the actual reflectance maximum in the final system would be shifted to shorter wavelengths, and this is exactly what we see in Fig. 3, showing the reflectance and transmission results for the completed multi-layer system, for both s- and p-polarizations. The new reflectance maximum is at ≈ 365 nm, with over 90% reflection between the wavelengths 350−370 nm (for s-polarization). Thus our system acts as a near-UV reflective filter.

We do nonlinear least-squares to find best-fit values for the thicknesses and densification factors, and the resulting curves for R and T are also drawn in Fig. 3. The discrepancies between the experimental data and theoretical best-fit curves are most likely due to the simplifications of the model; whereas in the actual stack, each of the ten TiO_2 and eight SiO_2 layers might have slightly different thicknesses, the model uses just two parameters, d_{TiO_2} and d_{SiO_2}, to describe the thickness of each type of layer. Similarly the densification factor D for each layer will vary depending

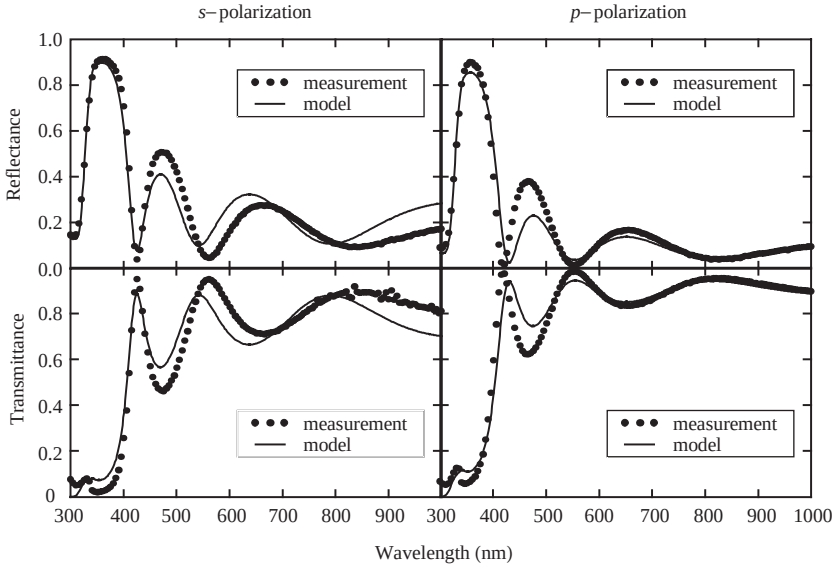

Fig. 3. The experimental reflectance and transmittance of the reflective filter system, for both the s- and p-polarizations (in the left and right-hand columns, respectively). The solid lines are the best-fit results of the model described in Section 2.

on the position of the layer in the stack; again the model distinguishes only two D factors, one for the TiO_2 and one for the SiO_2 layers. Clearly our model should give a better approximation when the same type of layer is repeated fewer times, and in fact for the AR filter system (where each layer type appears only twice, one on each side of the substrate), the theoretical curves fit the experimental results more closely, as will be seen in the next section. Despite our simplifications, the qualitative optical properties of the reflective filter are reproduced well, in particular the position and height of the reflectance maximum.

Fig. 4 shows the best-fit dispersion curves for the individual layer refractive indices and extinction coefficients. These results for n and k are consistent with physically accepted values for TiO_2 and SiO_2 films. The calculated model parameters are listed in Table 1. For comparison, we also show the thickness found from the single-layer data. As expected, the thickness of the layers in the stack are noticeably smaller. This accounts for the large shift in the reflectance peak.

Despite the relatively low temperature, 100 °C, used during the multiple heat treatments of this system, the stability of the resulting films does not seem to be adversely affected: a cross-cut and tape test found excellent adhesion (5B [26]).

4.2. AR filter

Figs. 5 and 6 show the experimental reflectance and transmittance results for the two AR filter systems, together with theoretical best-fit curves. The design of the two

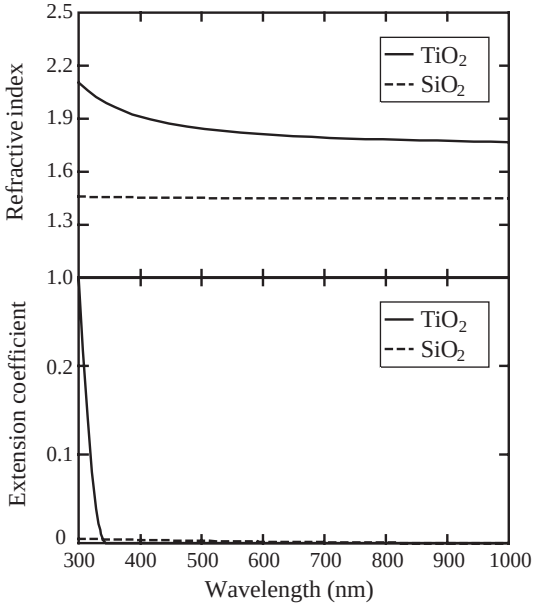

Fig. 4. Best-fit results for the refractive indices and extinction coefficients of the component layers in the reflective filter system.

Table 1
Best-fit results for the model parameters in the reflective filter system. For comparison, the bottom row lists the single-layer thickness results

Parameters	TiO_2	SiO_2
Densification factor D	1.04 ± 0.01	1.00
Thickness (in stack)	57.7 ± 1.2 nm	49.3 ± 2.2 nm
Thickness (single-layer)	66.3 ± 0.4 nm	86.7 ± 0.7 nm

filters differs in the relative thickness of the component layers (Type I using five sub-layers of TiO_2 versus 10 for Type II). In addition, the Type II system was fired at 450 °C after the coating process was complete. As with the reflective system, the choice of sol parameters was motivated by theoretical predictions using the thickness results from the single-layer samples. For the Type I system, the model indicated an AR minimum where the optical thickness of the three layers summed to $\lambda/2(k = 1)$. When we chose the sol parameters to position this minimum at $\lambda = 1050$ nm, based on the single-layer thickness, we found the final multi-layer system had shifted to a minimum near 805 nm, as seen in Fig. 5. In contrast, the Type II system has a broad W-shaped AR region, with the shorter-wavelength valley of the W centered at the λ

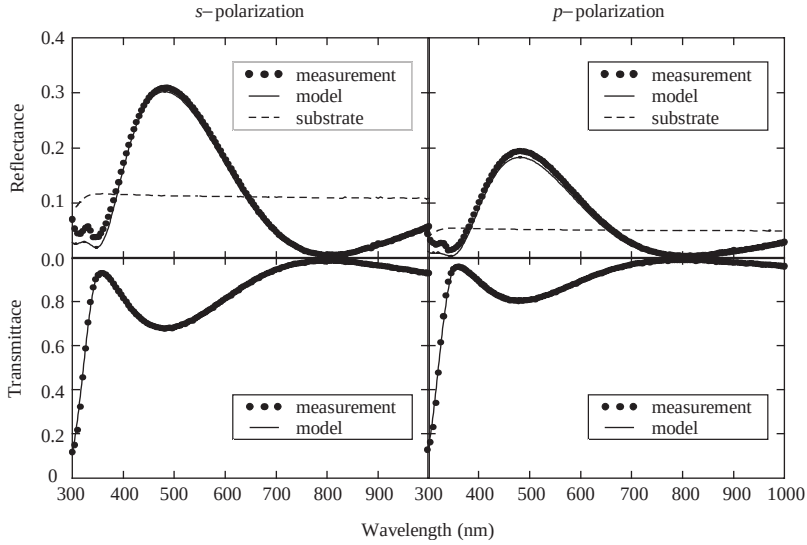

Fig. 5. The experimental reflectance and transmittance of the Type I AR filter system, for both the s- and p-polarizations (in the left and right-hand columns, respectively). The solid lines are the theoretical best-fit results.

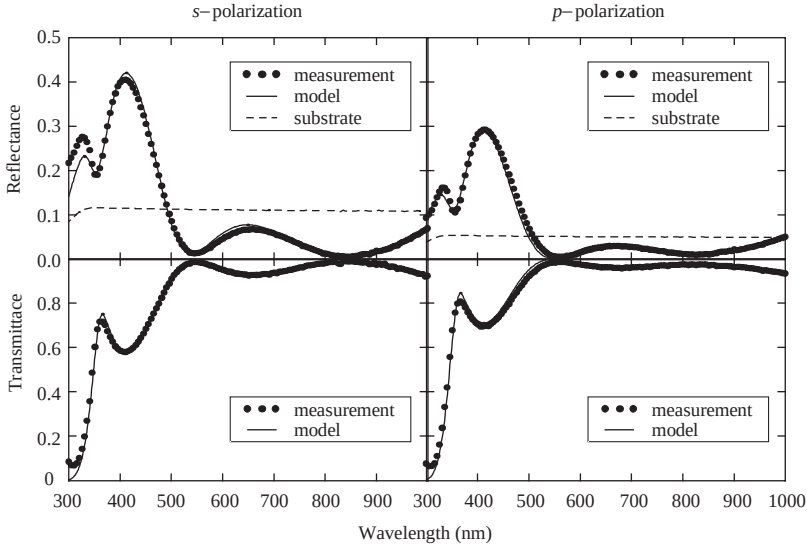

Fig. 6. The experimental reflectance and transmittance of the Type II AR filter system, for both the s- and p-polarizations (in the left and right-hand columns, respectively). The solid lines are the theoretical best-fit results.

where the optical thicknesses sum to $\lambda(k = 2)$. When we used the single-layer results and adjusted the sol parameters to place this valley at 595 nm, we found that in the final system it was near 545 nm. The shift between the predicted and observed spectra is significantly smaller for the Type II than for the Type I system, a fact which will be explained below when we discuss the significance of the final heat treatment temperature.

For the Type I system, the AR region is centered around $\lambda = 805$ nm. For wavelengths between 770−845 nm, the reflectance is less than 1%, while in a range 745−885 nm it is less than 2% (for the s-polarization). In comparison, the glass substrate has $\approx$ 11% reflectance. The Type II system has two local AR minima, at 545 and 845 nm, respectively. At 545 nm, the minimum reflectance is only 1.3%, and remains under 2% for a narrow range of 535−560 nm (for the s-polarization). The other minimum is deeper and broader, with the reflectance under 2% between 785−910 nm, and under 1% between 815−865 nm. Both systems can function as NIR AR filters.

From the shift between predicted and observed spectra mentioned above, we see that the single layer samples are a better predictor of stacked layer properties in the Type II system. We also see this in our best-fit results for the model parameters, which are listed in Table 2. The densification factors for the layers in the Type II filter are smaller than those of the corresponding layers in the Type I filter. (Remember the D factor measures relative densification: compared to the single layer sample, how much more dense is the same layer after it has been prepared as part of a multi-layer stack.) To explain these differences between the Type I and Type II filters, let us take a closer look at one of the layers, for example the TiO_2 which is the middle layer in the stack.

We start with the TiO_2 layer in the Type I filter. The associated single layer sample is prepared by coating 5 sublayers of TiO_2 on the substrate, and keeping each sublayer in the oven for 5 min at 100 °C. When we construct the multi-layer stack, the TiO_2 layer is prepared in exactly the same way, but by the end of the fabrication process it has spent more time in the furnace (because we added an SiO_2 layer on top and heat-treated it). The densification factor D is a measure of what effect this extra

Table 2
Best-fit results for the model parameters in the AR filter systems. For comparison, the single-layer thickness results are also shown

Type I			
Parameters	TiO_2–SiO_2	TiO_2	SiO_2
Densification factor D	1.30 ± 0.06	1.04 ± 0.01	1.004 ± 0.008
Thickness (in stack)	25.7 ± 3.0 nm	55.5 ± 3.2 nm	168.5 ± 2.1 nm
Thickness (single-layer)	65.9 ± 1.2 nm	106.8 ± 0.2 nm	182.4 ± 1.2 nm
Type II			
Densification factor D	1.17 ± 0.06	1.001 ± 0.002	1.00
Thickness (in stack)	32.1 ± 3.9 nm	137.4 ± 2.1 nm	131.9 ± 0.7 nm
Thickness (single-layer)	44.7 ± 1.8 nm	143.4 ± 0.3 nm	147.7 ± 1.0 nm

furnace time has on the index of refraction of TiO_2. At the relatively low temperature of 100 °C, we expect densification to proceed slowly: the heat treatment during the coating of the TiO_2 layer will not have completely removed all the residuals of the sol–gel synthesis, and the extra furnace time during the coating of the top layer will continue the densification process for the TiO_2 layer. Thus the TiO_2 layer in the finished stack is denser than the one in the single layer sample: we get a D factor of 1.04 ± 0.01.

Compare this to the TiO_2 layer in the Type II AR filter. The preparation of the single layer sample involves the same 100 °C heat treatment after each sublayer, but at the end we heat-treat it for 15 min at 450 °C followed by 8 min at 230 °C. Similarly after we construct the multi-layer stack, we take the finished stack and heat-treat it for 15 min at 450 °C followed by 8 min at 230 °C. At temperatures of 450 °C we expect onset of crystallization of TiO_2. The residuals of sol–gel synthesis will be rapidly evaporated or burned off, and the film will eventually achieve a stable thickness. It should not make much difference whether beforehand the film was exposed to longer furnace times at 100 °C: during the subsequent 450 °C heat treatment, the TiO_2 in the single layer sample and the TiO_2 in the stack should both approach some final, stable density for the crystallized film. In fact we get a D factor of 1.001 ± 0.002, less than the D for TiO_2 in the Type I filter.

In general because of rapid densification at higher temperatures, we expect the D factors for layers in the Type II filter to be smaller than their counterparts in the Type I filter, and this is exactly what we see in the Table 2 results. In addition we find another pattern agreeing with our intuition: the lower layers spend longer times in the furnace (compared to their corresponding single layer samples) than the higher layers, and thus the densification factors are greatest for the bottom layer (the TiO_2–SiO_2 mix), and decrease as we go up. The top layer in the stack (SiO_2) should have a D factor approximately equal to 1, since it undergoes exactly the same heat treatment as its corresponding single layer sample.

There is a recent study by A. Díaz-Parralejo et. al. [27], which supports the above observations. The authors looked at densification of ZrO_2−3 mol% Y_2O_3 sol–gel thin films using heat treatments at a variety of temperatures. Among their results they found that for the low temperature regime (100–200 °C) the total duration of heat treatment has a noticeable effect on film thickness (densification occurs slowly, so the thickness of the film continues to decrease with longer furnace times); while in the intermediate regime (300–500 °C), once crystallization sets in, extending the heating time has little or no influence, since the film thickness has achieved an approximately constant value.

The calculated best-fit refractive indices and extinction coefficients for the two types of AR filter are shown in Fig. 7. For the Type I system, the densification of the mixed TiO_2–SiO_2 at the bottom of the stack is large enough to increase its refractive index as high as the index of the pure TiO_2 layer. The two bottom layers effectively become a single high-index layer, thus explaining some of the difference between the optical properties of the two systems (which share the same layer sequence).

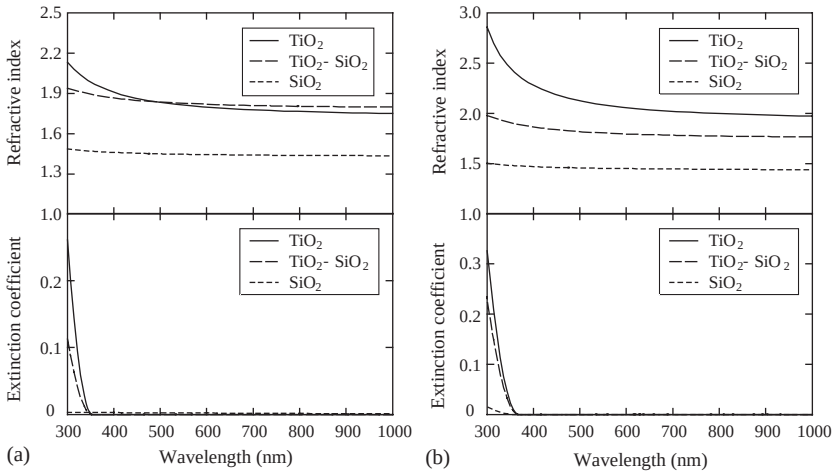

Fig. 7. Best-fit results for the refractive indices and extinction coefficients of the component layers in the AR filter systems: (a) Type I and (b) Type II.

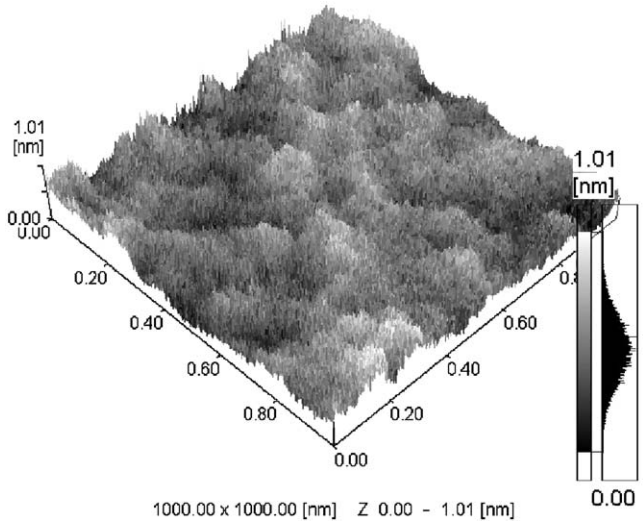

Fig. 8. AFM surface measurement for the Type I AR system.

As in the case of the reflective filter, even the heat treatment at 100 °C seemed sufficient to produce stable films: both the Type I and Type II coatings had excellent adhesion under the cross-cut and tape test (5B [26]). Our thin films also have very smooth surfaces, seen in the AFM results of Figs. 8 and 9 for the Type I and Type II systems, indicating average roughness of a few nanometers.

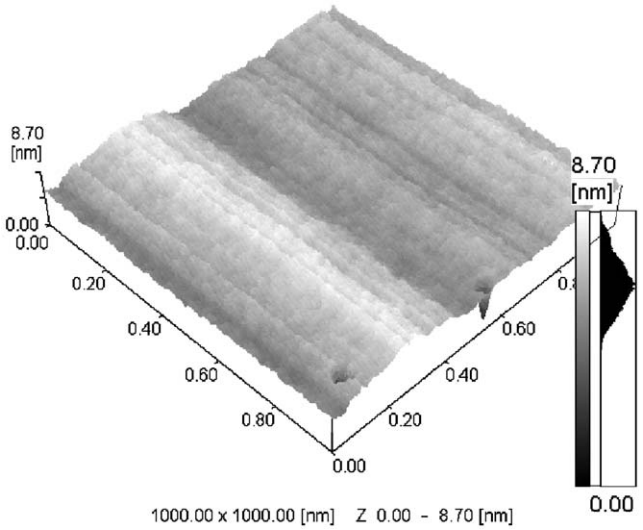

Fig. 9. AFM surface measurement for the Type II AR system.

5. Conclusion

Thin film systems using both the sides of a substrate through the sol–gel spin-coating technique can be designed for a variety of useful purposes, of which the near UV reflective and near-infrared (NIR) anti-reflective (AR) filters described in this study are only a few. Choosing a layer arrangement to give the system some desired reflectance or transmittance profile requires an effective theoretical model, one that can account for the often-complex changes of sol–gel thin films during the coating process. The model presented here is tailored specifically to the task of sol–gel multi-layers involving a few basic layer types from which the entire sequence is created. By associating a small number of free parameters to each layer, we can model the optical properties of even a fairly large sequence.

Acknowledgements

The authors are thankful to E.D. Sam and E. Arpat for their kind help in the cross-cut and tape tests. We also thank E. Pehlivan for the AFM measurements and other assistance, and are grateful to K. Koç, I. Turhan, E. Özkan Zayim, and I. Sorar for many useful discussions. The Turkish State Planning Organization has generously supported this research.

References

[1] R.M. Almeida, A.S. Rodrigues, J. Non-Cryst. Solids 326&327 (2003) 405–409.
[2] R.M. Almedia, S. Portal, Curr. Opin. Solid State Mater. Sci. 7 (2003) 151–157.

[3] R.M. Almeida, Z. Wang, Proceedings of the SPIE, 2002, pp. 24–33.
[4] V. Kozhukharov, Ch. Trapalis, B. Samuneva, E. Kirilova, J. Mater. Sci. Lett. 11 (1992) 1206–1208.
[5] P.K. Biswas, D. Kundu, D. Ganguli, J. Mater. Sci. Lett. 6 (1987) 1481–1482.
[6] C.C. Trapalis, M.A. Karakassides, G. Kordas, X. Aslanoglou, Mater. Lett. 25 (1995) 265–269.
[7] D. Kundu, P.K. Biswas, D. Ganguli, J. Non-Cryst. Solids 110 (1989) 13–16.
[8] K.M. Chen, A.W. Sparks, H.-C. Luan, D.R. Lim, K. Wada, C. Kimerling, Appl. Phys. Lett. 75 (1999) 3805–3807.
[9] S. Rabaste, J. Bellessa, C. Bovier, J.C. Plenet, R. Brenier, O. Marty, J. Mugnier, J. Dumas, Thin Solid Films 416 (2002) 242–247.
[10] Q. Zhang, X. Li, J. Shen, G. Wu, J. Wang, L. Chen, Mater. Lett. 45 (2000) 311–314.
[11] M. Mennig, P.W. Oliveira, A. Frantzen, H. Schmidt, Thin Solid Films 351 (1999) 225–229.
[12] Q. Zhang, J. Wang, G. Wu, J. Shen, S. Buddhudu, Mater. Chem. Phys. 72 (2001) 56–59.
[13] M. Mennig, P.W. Oliveira, H. Schmidt, Thin Solid Films 351 (1999) 99–102.
[14] G. San Vicente, A. Morales, M.T. Gutierrez, Thin Solid Films 391 (2001) 133–137.
[15] E. Hammarberg, A. Roos, Thin Solid Films 442 (2003) 222–226.
[16] M.C. Bautista, A. Morales, Sol. Energy Mater. Sol. Cells 80 (2003) 217–225.
[17] M.S.W. Vong, P.A. Sermon, Thin Solid Films 293 (1997) 185–195.
[18] P. Nostell, A. Roos, B. Karlsson, Thin Solid Films 351 (1999) 170–175.
[19] G. San Vicente, A. Morales, M.T. Gutierrez, Thin Solid Films 403&404 (2002) 335–338.
[20] F.L. Pedrotti, L.S. Pedrotti, Introduction to Optics, Prentice-Hall, London, 1993, p. 392.
[21] S.H. Wemple, M. DeDomenico, Phys. Rev. B 3 (1974) 1338–1351.
[22] R. Capan, N.B. Chaure, A.K. Hassan, A.K. Ray, Semicond. Sci. Technol. 19 (2004) 198–202.
[23] J. Tauc, Amorphous and Liquid Semiconductors, Plenum, New York, 1974, p. 159.
[24] A.M. Seco, M.C. Conçalves, R.M. Almeida, Mater. Sci. Eng. B 76 (2000) 193–199.
[25] M. Born, E. Wolf, Principles of Optics, Pergamon Press, Oxford, 1987.
[26] ASTM D3359-02.
[27] A. Díaz-Parralejo, R. Caruso, A.L. Ortiz, F. Guiberteau, Thin Solid Films 458 (2004) 92–97.